Chapter- 6

Fluid Flow Analysis of TPMS Unit Cells

6.1 Introduction to behaviour of porous cells in tissue engineering application

Fluid flow characteristics of porous scaffolds are essential in bone regeneration for delivering necessary nutrients to cells and managing scaffold biocompatibility. The bioactivity of scaffold is governed by features like as permeable behaviour and wall shear stress (WSS) caused by fluid flows. The oxygen and nutrition supply via the porous media is essential for biological properties, and shear stresses caused by fluid flow are regarded as the major mechanical stimuli for cell growth and maturation in scaffold (Mahammod et al. 2020). Development of new blood-vessel is essential for tissues to develop beyond 100–200 m (the oxygen diffusion limit) (Carmeliet and Jain 2000). In perfusion bioreactors, for example, large surface constructions could easily get nutrients by in vitro cultivation (Janssen et al. 2006). But when tissue constructions have been implanted, diffusion mechanisms which could only support cells up to 100 to 200 micrometres from the next capillary frequently restrict the amount of oxygen and nutrition which could reach the implant. The tissue needs to be vascularized, meaning that capillary system needed to transport nutrition to cells is established inside the tissues, for larger transplanted tissues to survive. In general, blood arteries from the hosts penetrate the tissues following implantation to develop this network, partly owing to signals generated by transplanted cells being sensitive to hypoxia (Rouwkema et al. 2008).

The amount of time required to completely vascularize any implant measuring few millimetres is on the order of weeks because such spontaneously occurring vascular ingrowth can sometimes be restricted to the few tenths of micrometres in a day (Clark and Clark 2005). Inadequate vascularisation at such stage might result in nutritional deficits and may lead to hypoxia. Furthermore, oxygen and nutrition imbalances might exist in the tissue's periphery, that might lead to ineffective cell division and adhesion, consequently reducing tissue regeneration (Malda et al. 2004).

Mironov et al. employed an advanced manufacturing technology depending on organ manufacturing of tissue spheroids as basic components for the bioprinting of live organ constituted of the functioning tissues and internal branching vascular system to address this issue (Mironov et al. 2009). Tissue fusion occurs between closely positioned tissue spheroids, representing a basic cellular basis of biophysically controlled tissue self-assembly. Individual portions of an intra-organ branching vascular structure can be constructed utilising solid and lumenized vascular tissue spheroids. The ability to create an organ with complete vascularization is made feasible by employing two different kinds of spheroids, one for the vascular tree and the other for the organ tissue. to be used in the biofabrication of vascularized organs. Skin or cartilage are examples of thin, avascular tissues where the needs for oxygen and nutrients can be met by the host's post-implantation neovascularization, are now the only tissues for which tissue-engineered structures are successfully used since the speed of vascularization after implantation is a key difficulty in tissue engineering (Jain et al. 2005). To successfully apply tissue engineering to larger tissues like bones and muscles, the difficulty in vascularisation must be overcome (Johnson et al. 2007).

6.2 Problem Definition

It is essential for biological fluid to permeate through the scaffolds in order to supply the cells with nutrition, oxygen, and a way to flushing away waste products of metabolism (Vossenberg et al. 2009). The flow pattern determines the effectiveness of cell adhesion to the scaffolds. Heavy flow lead to higher shear stresses, that limits cell adhesion to the surfaces of scaffolds. Cells that have already adhered may be destroyed or their ability to proliferate is inhibited (Martin and Vermette 2005). For in vivo systems, shear stress is regarded as another crucial component. In an investigation, Wang and Tarbell (Wang and Tarbell 2000) revealed that the synthesis of prostaglandins enhanced for smooth muscle cells with increased shear stresses.

Wang and Tarbell's findings suggest that blood flow rate is vital in the signal transmission pathway from blood arteries to smooth muscle cells.

The shear stresses that affect the scaffold fibres, upon which cells are formed, needs to be taken into account while developing the scaffold. Shear stresses are the result of design characteristics like fibre diameter and distances among fibre center as well as operational variable like flow rate and is proportional to the velocity gradients. In bioreactors or other in vitro systems, the cells are exposed to a constant nutritional fluid velocity. The fluidic movement is shown to cause stresses on the cells adhering to the wall of scaffold, known as wall shear stress. When the wall shear stress is too severe, it may gradually detach the connected cells and destroy them, this reduces the capacity of cells to adhere to the scaffold walls. Additionally, lower levels will not provide the essential stimulation for appropriate cell growth and development. To put it another way, every single cell has its own shear stress level. The impact of shear stress on optimal, critical, or even fatal levels for various cultured cells in bioreactor has already been addressed by a number of researchers. (Martin and Vermette 2005, Godara et al. 2008, Park et al. 2008, Radisic et al. 2008, Porter et al. 2005, Cartmell et al. 2003, Schinagl et al. 1999).

Additionally, scaffold structures with greater pore interconnectivity and porosity are more suitable for nutrient transportation and vascularization. vessels. It is essential to use the CFD approach to explore the fluid flow characteristics and response, since they are vital for 3D vascular cell culture. The fluid response of the scaffolds may be optimized depending on CFD simulations for generating adequate structural stability, higher permeability, and optimal cell adhesion and growth under flow field. Previous research employed CFD to model and compute the fluid movement profiles, fluid velocities, pressures, permeability, WSS, shear strains, and availability of oxygen. In this chapter we were focused on the fluidic behaviour of those structures which has performed well in morphological and mechanical evaluation in

contrast to the bone properties. Thus, the gyroid and primitive with some particular ranges of porosities has performed well. However, to show the variations in permeability and WSS we have included 5 porosity level from 50% to 90% in the fluidic behaviour study.

6.3 TPMS unit cell fluidic behaviour simulation

Evaluating the permeability on the scaffold surface and the porosity dependency on wall shear stress is the major objective of the unit cell performance simulation. The efficiency of the cell in terms of its ability to proliferate and differentiate both at internal and external levels throughout the porous structure is affected by these two factors, making them the most important.

Obtaining a geometrical representation of the fluid that is already there, or the voids inside the scaffold unit, as illustrated in Figure 6.1, is the initial stage if the scaffold is contained inside fluidic surroundings. Flow simulations allow for the analysis of fluid flow rate, pressure drop, and flow velocity for various scaffold structures. As illustrated in Figure 6.2, the unit cell was developed with a design that had a two-unit vertical length enclosed to simulate the fluid already available.

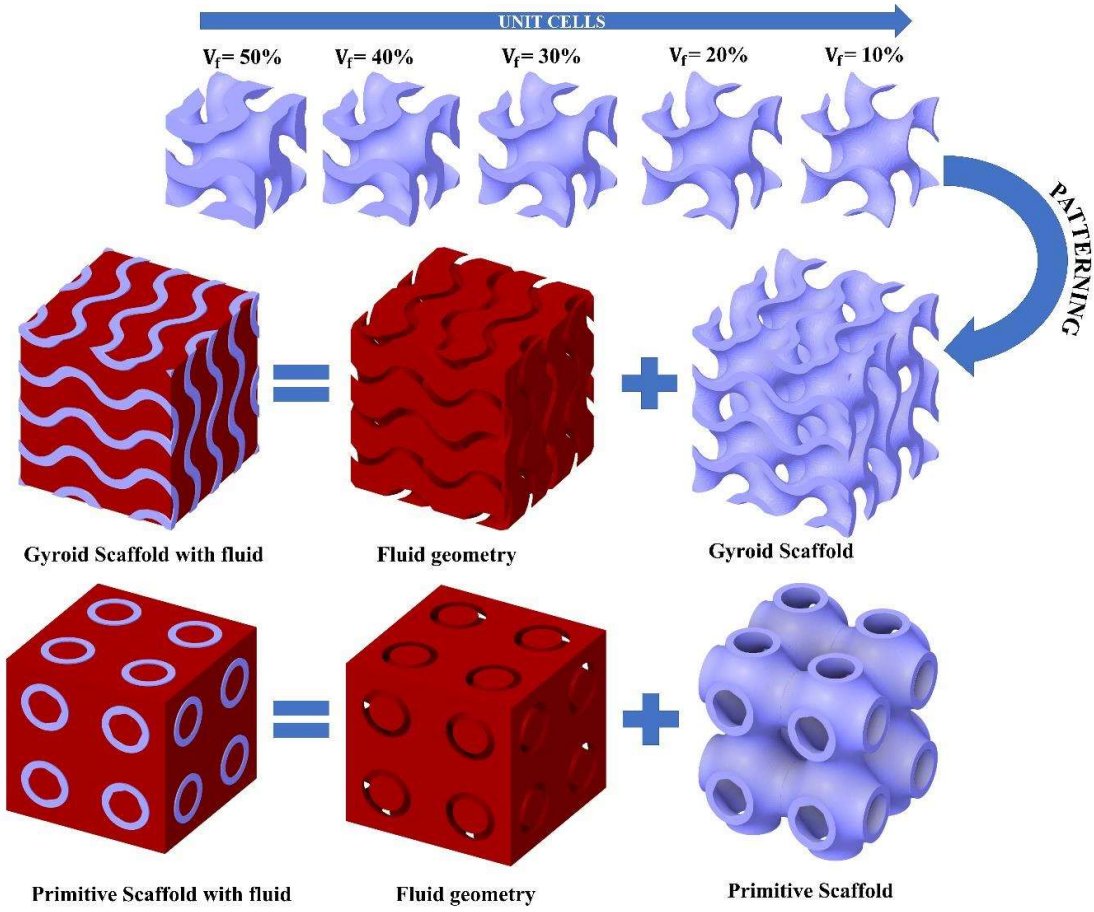

Figure 6.1: Illustration of gyroid and primitive TPMS unit cells with varying volume fraction which is uniquely patterned in X, and Z coordinate to take desired shape of lattice or scaffold. An interpenetrating fluid phase is created by subtracting the solid volume with the volume of lattice. Similarly illustrated, primitive scaffold of varying volume fraction from 10% to 50% is included in this study.

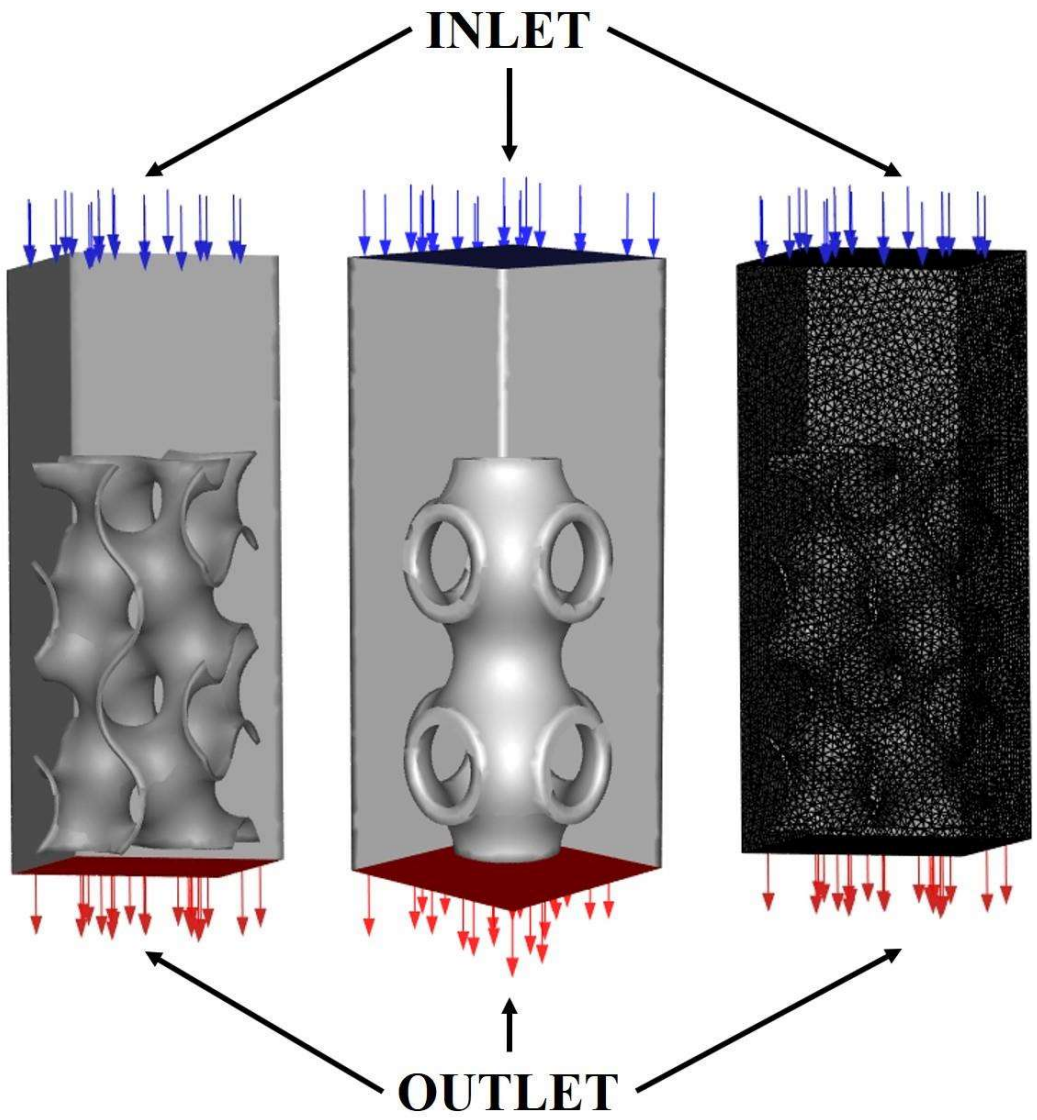

Figure 6.2: Modelling domains represented as grey (solid) and pink (fluid) for (left) Gyroid and (middle) Primitive (right) Illustration of mesh for TPMS and fluid geometry.

6.4 Boundary conditions and Governing equations in CFD analysis

In this work, for incompressible flow mechanics the Navier-Stokes equation was adopted (Vossenberg et al. 2009). The relation is expressed below as:

$$\rho \frac{\partial u}{\partial t} - \mu \nabla^2 u + \rho(u.\nabla)u + \nabla p = F, \qquad \nabla.u = 0 \tag{6.1}$$

Where, ρ represents fluid density (kg/m^3), u represents fluid flow velocity (m/s), μ shows fluid dynamic Viscosity (kg/m.s), "∇ " represents Del operator, p shows pressure (Pa) and F shows additional forces like gravitational/centrifugal forces. Here, the value of F is assumed as zero (Vossenberg et al. 2009).

Water was considered as the fluid for evaluation due to its simplicity (Martin and Vermette 2005). As a result, the physical parameters of water (density 1000 and viscosity 0.001PaS) were applied to fluid domain of CFD model simulations.

Using Darcy's law as a basis (Truscello et al. 2012), permeability (k) was calculated as follows:

$$k=\frac{Q\mu L}{A\,\Delta P} \tag{6.2}$$

where, Q defines the rate of fluid flow (m^3/s); μ shows viscosity of fluid (kg/m.s), L is length of model (mm), A is unit cell cross-sectional area (mm^2), and ΔP is and pressure drop (Pa), correspondingly.

It is possible to define the normal velocity gradients on the wall as wall shear stress τ_ω representing Newtonian fluid in a laminar systems (Egger et al. 2017):

$$\tau_\omega=\mu\frac{\partial V}{\partial n} \tag{6.3}$$

Where, μ represents dynamic viscosity; V is the velocity of flow; and n shows x, y, and z directions.

During the CFD study, 0.1 mm/s of velocity was applied at inlet (Truscello et al. 2012, Voronov et al. 2010), hydrophilic surfaces were considered for scaffold, and no-slip constraint was implemented at wall surfaces (Lesman et al. 2010m, Marin and Lacroix 2015, Truscello et al. 2012). Because of the models' repeated designs and the requirement to prevent lengthy simulations, mainly two-unit cells were included in the CFD study (Truscello et al., 2012).

Figure 6.2 shows the boundary conditions applied at fluid domains of scaffold two unit cells as an example.

6.5 Convergence and Solutions

Predictions of the pressure as well as WSS inside the scaffold were made using Ansys Fluent. Tetrahedral elements were used to mesh the models' fluid domain (Gómez et al. 2016). The residual criteria value of 0.05 mm was used in the CFD simulation for convergence of results. Table 6.1 displays the number of elements for every model.

Table 6.1: Number of elements generated in each structure.

Structure	**Gyroid (G)**					**Primitive (P)**				
Porosity (%)	50	60	70	80	90	50	60	70	80	90
Number of elements	467107	437534	318136	374870	317356	204817	201610	186683	185524	189877

6.6 Fluid flow mechanism of porous scaffolds

Figures 6.3 and 6.4 show the vector and contour of velocity as well as pressure distribution modes for the Gyroid and Primitive models, respectively.

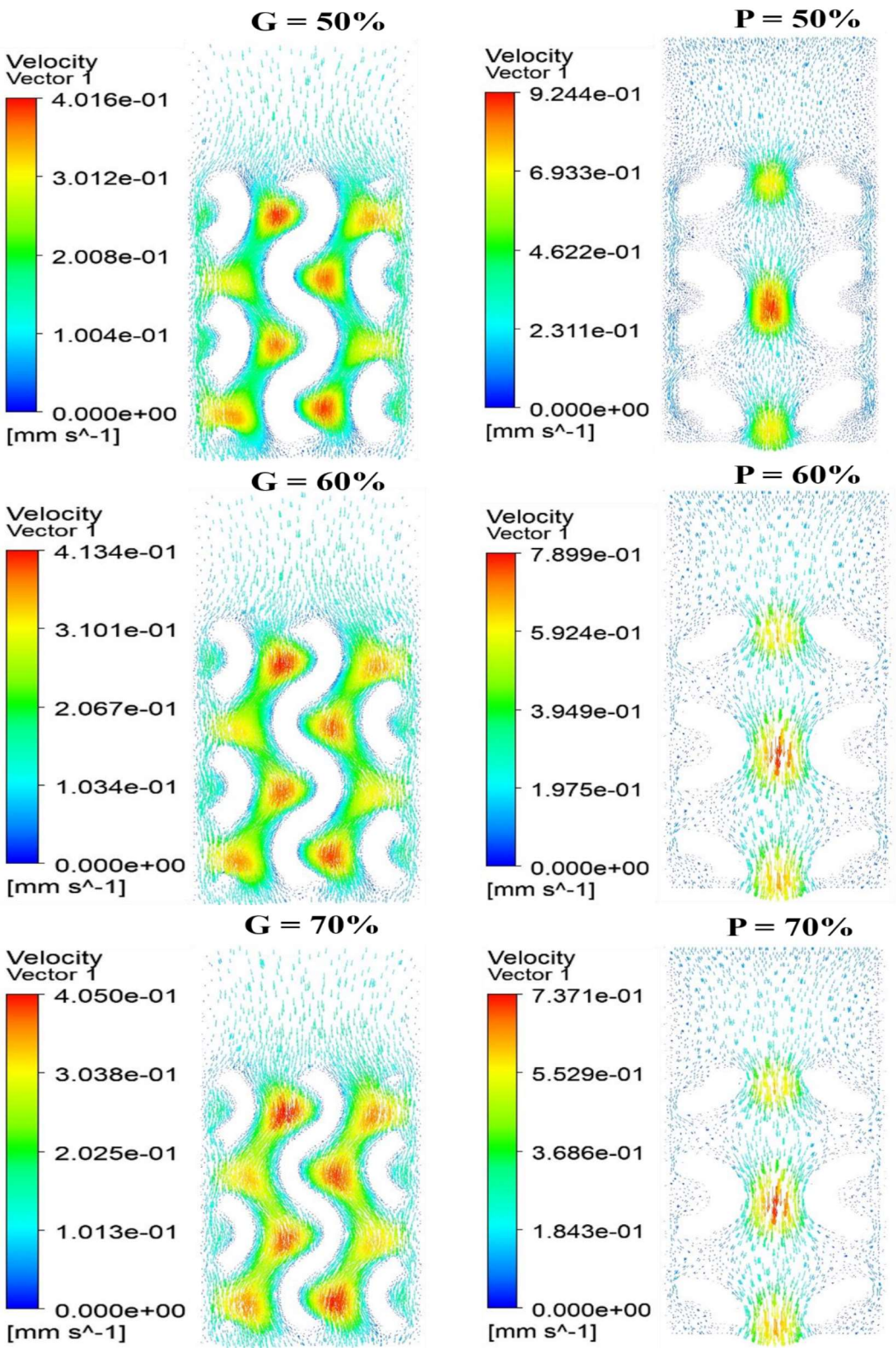

Figure 6.3: Velocity vectors at inlet velocity of 0.1 mm/sec; left column is for gyroid and right is for primitive.

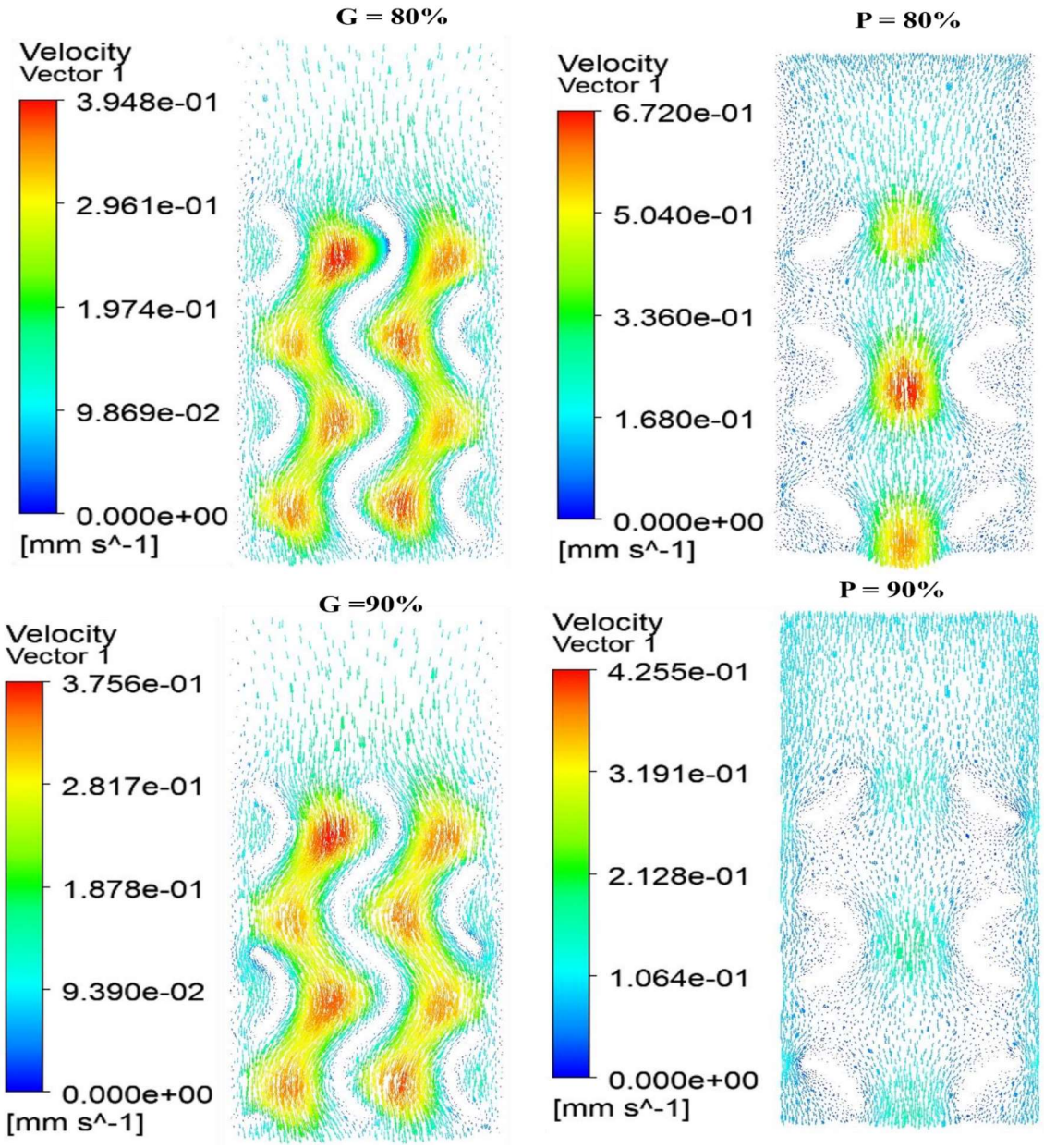

Figure 6.3: Continued

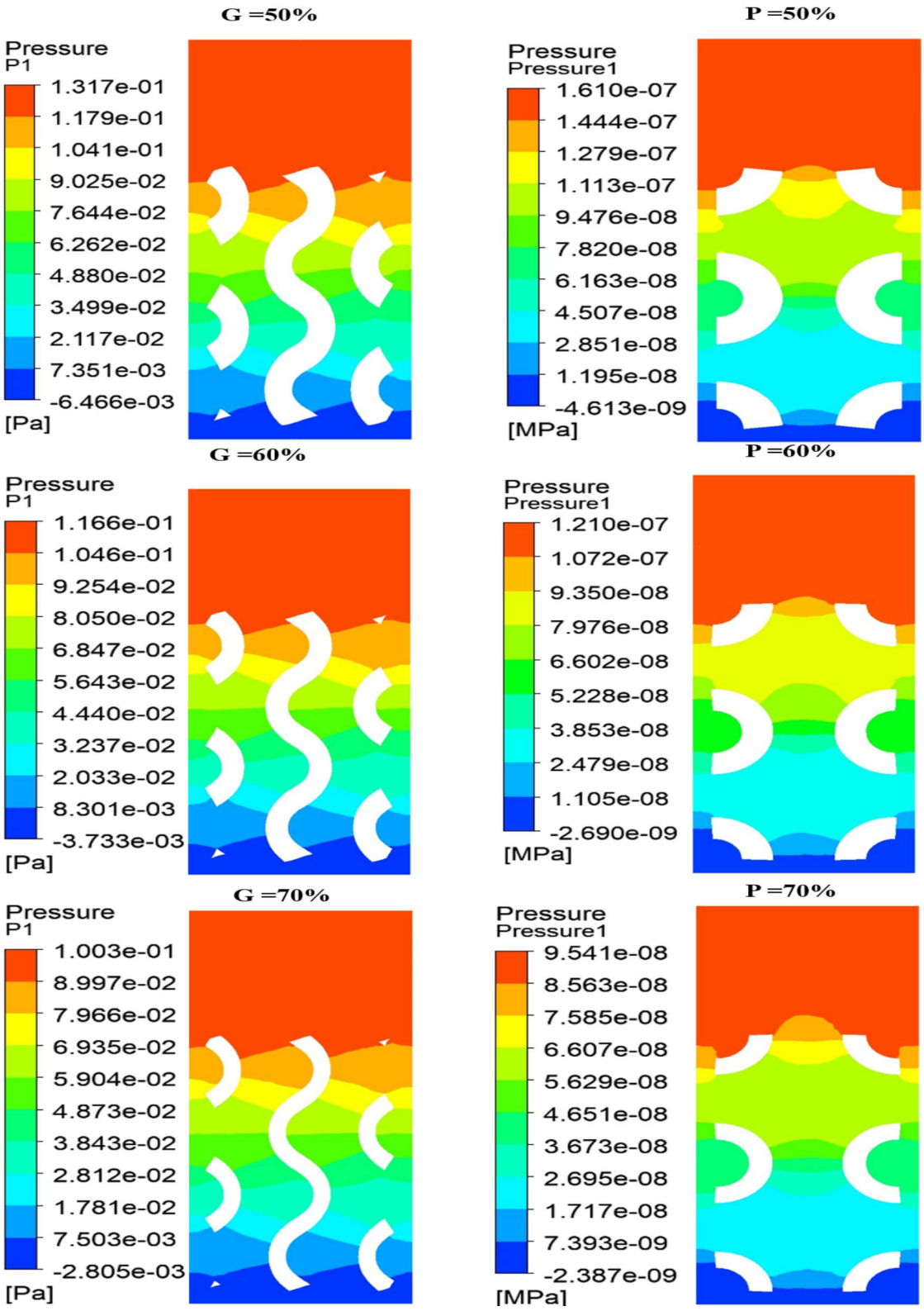

Figure 6.4: Pressure contour at inlet velocity of 0.1 mm/sec; left column is for gyroid and right is for primitive.

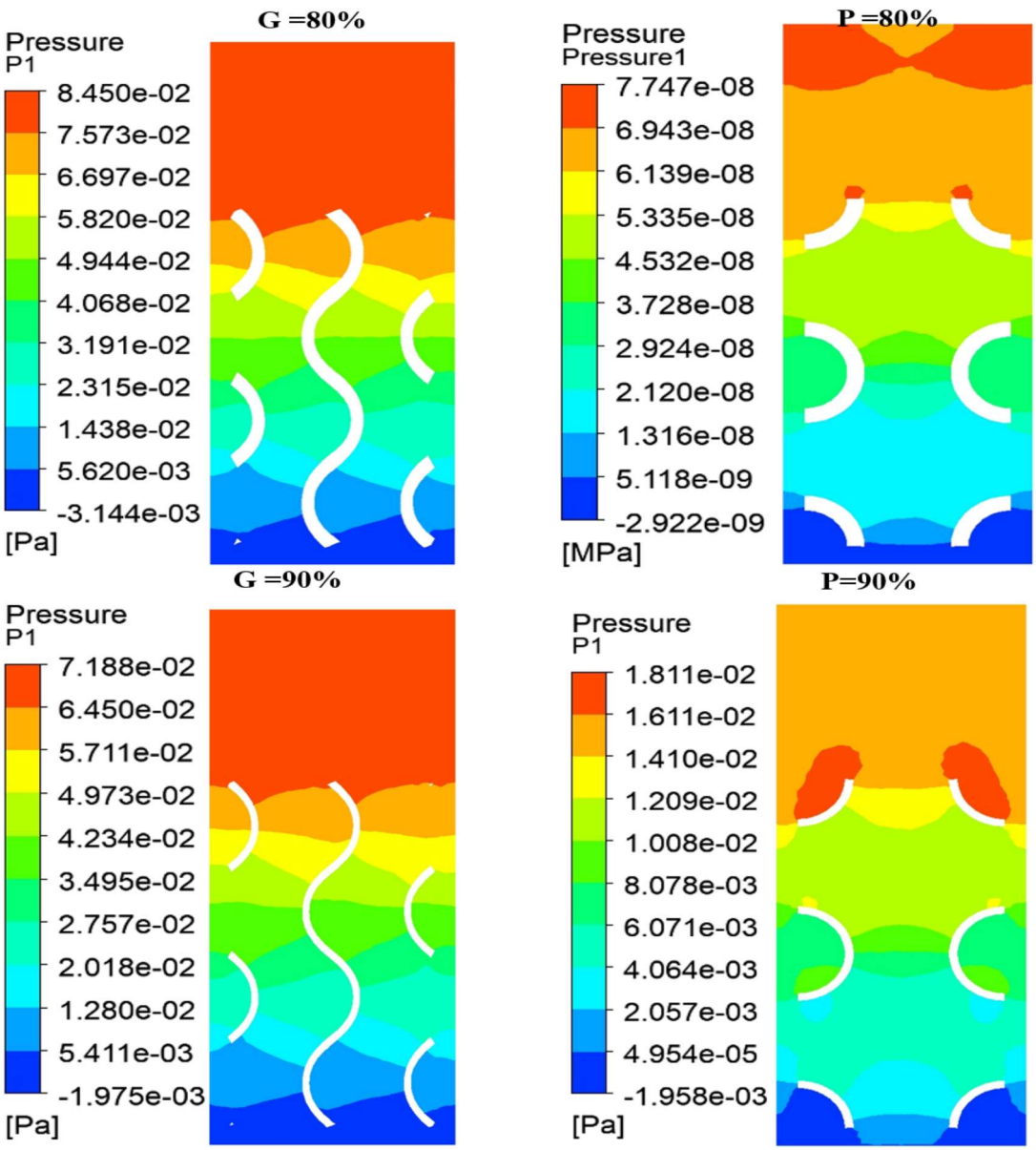

Figure 6.4: Continued

6.7 Results and Discussion

Figures 6.5 demonstrates the contours of the WSS in structure with increasing porosity and pore sizes. The contour of WSS indicate that there is no noteworthy apparent fluctuation at the inside layer, so the greater readings of WSS are found on the outer layer of both scaffolds in all porosity levels. In contrast to cells inside the scaffolds, the cells interacting with the

scaffold's external surface will experience high levels of mechanobiological stimulations. As a result of the absence of stimulation, the scaffold will experience lower levels of cell growth and differentiation. Additionally, on a macro-scale level, both the structures have a similar decreasing trend on increase of porosity, the decreasing trends can also be observed in Figure 6.6. However, the primitive structures have shown a higher trend in comparison to gyroid structures in all the porosity level. Considering that the WSS to be dependent on the velocity gradients as well (Equation 6.3), it can be concluded that the velocity gradients of fluid in scaffold having larger pore sizes were greater as compares to those having smaller pore sizes (Figure 6.3). WSS of the gyroid model was likewise lower than the Primitive model. Due of the convoluted structures of the Gyroid structures, fluid accelerations in this observation can be explained (Figure 6.6).

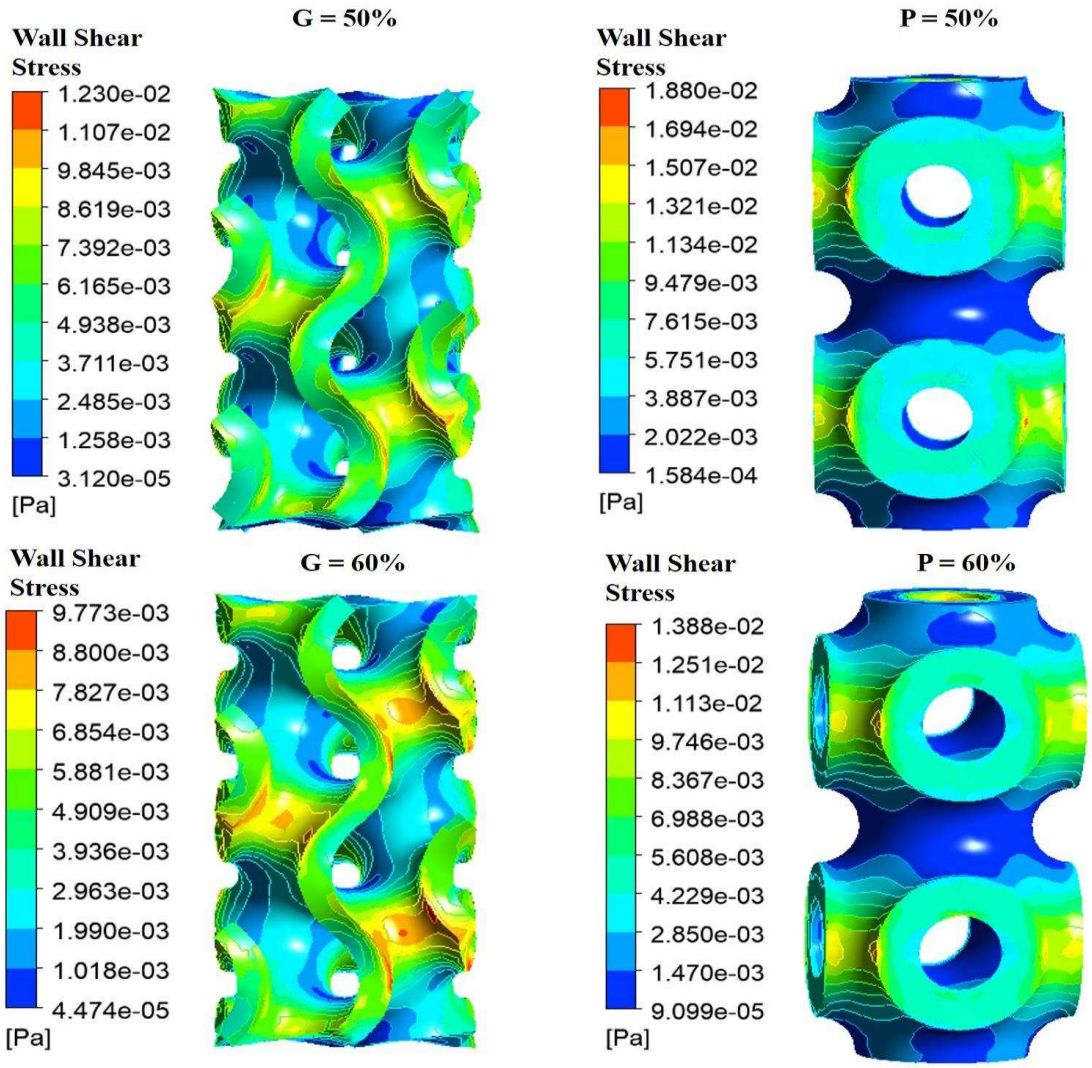

Figure 6.5: Variations in Wall Shear Stress with the change in porosity. left column is for gyroid and right column is for primitive.

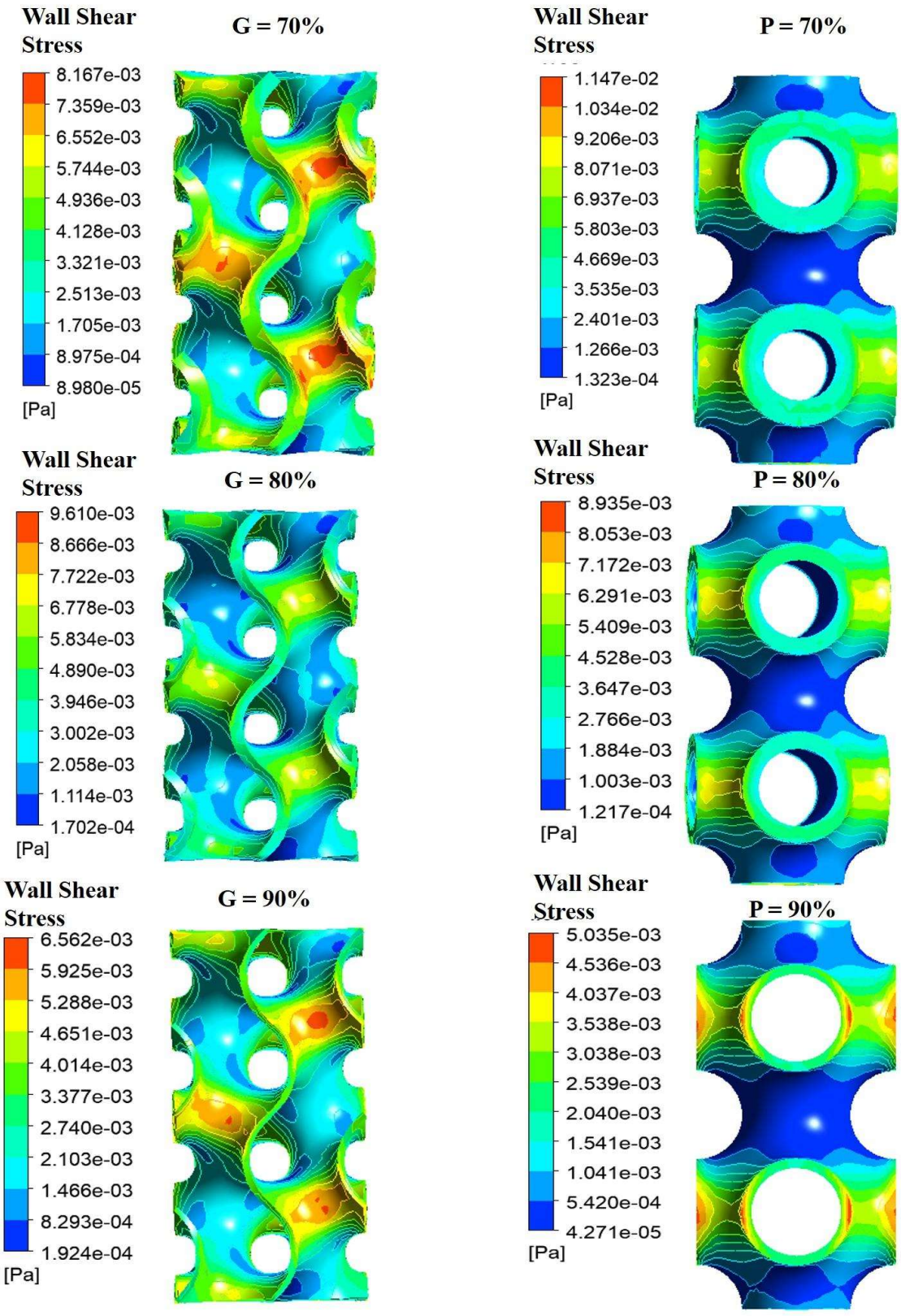

Figure 6.5: Continued

6.8 Permeability

Equation 6.2 and the resultant models were used to evaluate the permeability of CFD model. Figures 6.7 and 6.9 show the estimated permeability of total structures having input velocity of 0.1 mm/sec. Permeability improved as the scaffold pore size expanded (Figure 6.7). The primitive model's permeability was significantly lower than that of the gyroid models for same pore sizes. Model with pore size of 218 µm the gyroid model have the permeability of $32.64E^{-9}$ m^2 and primitive have $18.8E^{-9}$ m^2 which is highest among all pore size and porosity level. The reason for these variations is because the gyroid structures had no obstructions that prevented fluid transport. Consequently, lower pressure drop was experienced than those in Gyroid structures that are defined by more tortuous passages. The permeability value of the structures was accorded with those determined in study of Van Bael et al. to confirm the CFD result (Van Bael et al. 2012). There was quite strong and positive correlation in both the findings, with an inaccuracy of 1.8 %.

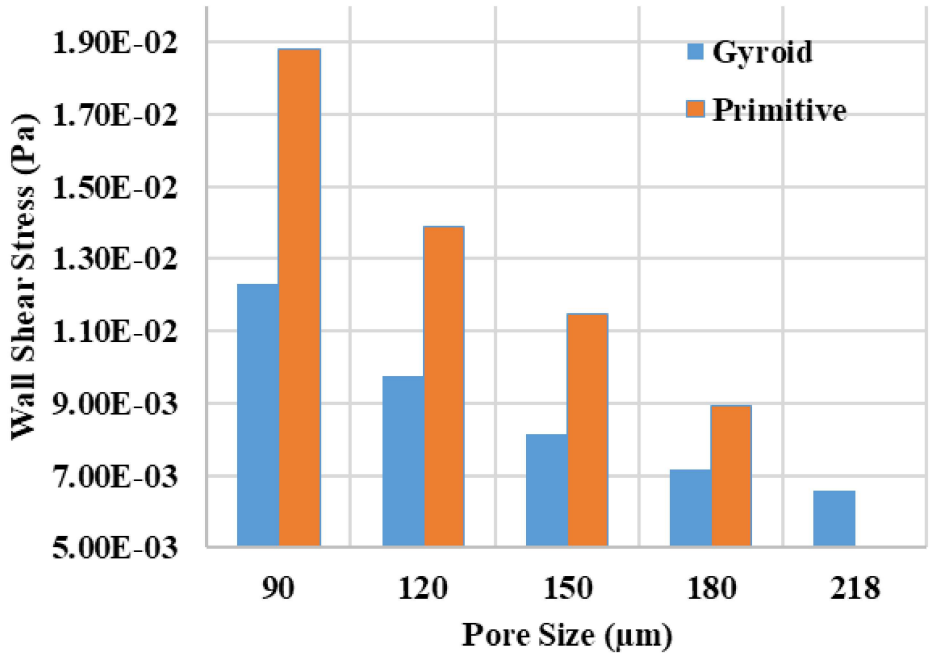

Figure 6.6: Average WSS with a velocity of 0.1 mm/sec in all the models.

WSS decreased with increased porosity, in contrast to permeability. Since the WSS was velocity gradient-dependent (Equation 6.3), it was concluded as velocity gradients of fluids in scaffold having smaller pore sizes were greater compared to those having larger pore sizes. WSS of the Gyroid models was likewise lower than that of the Primitive models. Due of the tortuous structures of the Gyroid models, fluid acceleration in this observation can be attributed (Figure 6.6).

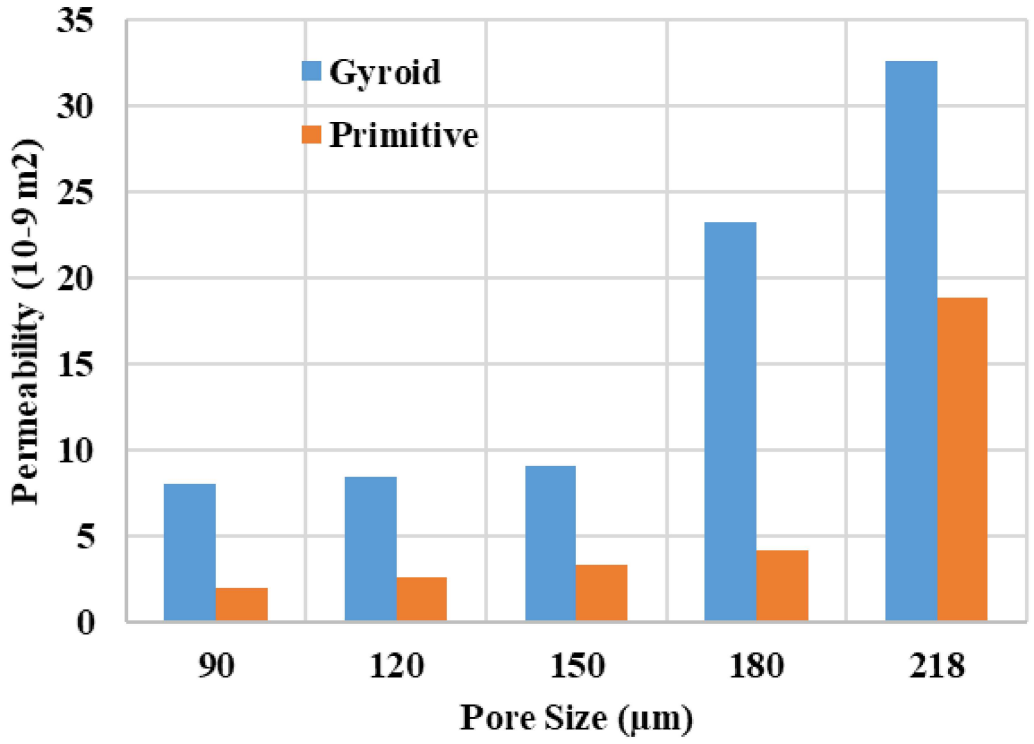

Figure 6.7: Average permeability with 0.1 mm/sec velocity in total developed models.

Although, ranges below 15 MPa are frequently advised for WSS for converting osteoblast as well as osteocyte obtained by mesenchymal stem cell within bioreactor systems. The otcomes are in excellent accord with this documented literature (Li et al. 2009, Olivares et al. 2009, Zhao, et al. 2015). Additionally, Permeability and WSS is also plotted in respect of thickness as shown in Figures 6.8 and 6.9. Permeability shown a gradual decrease with the thickness increase as shown in Figure 6.9. The lowest permeability in gyroid was obtained with

a thickness of 161 µm, whereas in primitive it was recorded with a thickness of 221 µm. It was an obvious increase in WSS with the increase in thickness. To which, primitive model of thickness 221 µm has shown the highest whereas at 42 µm it was the lowest. A similar trend can also be observed in the gyroid model as seen in Figure 6.8. However, a similar pattern was not observed between both the models at different porosity levels, which might be due to mesh dependency at a very smaller scale. It should be noted that the analyses in this work were performed by presuming water as a fluid medium. For in vitro settings, fluid containing cells might exhibit viscosity behavior differing from that of water. This is a factor that might alter pressure drops and WSS values. For cell culture with 5% wt/wt dextran, Sinha et al. estimated the value of 0.0037 kg/m-s for viscosity (Sinha et al. 2016).

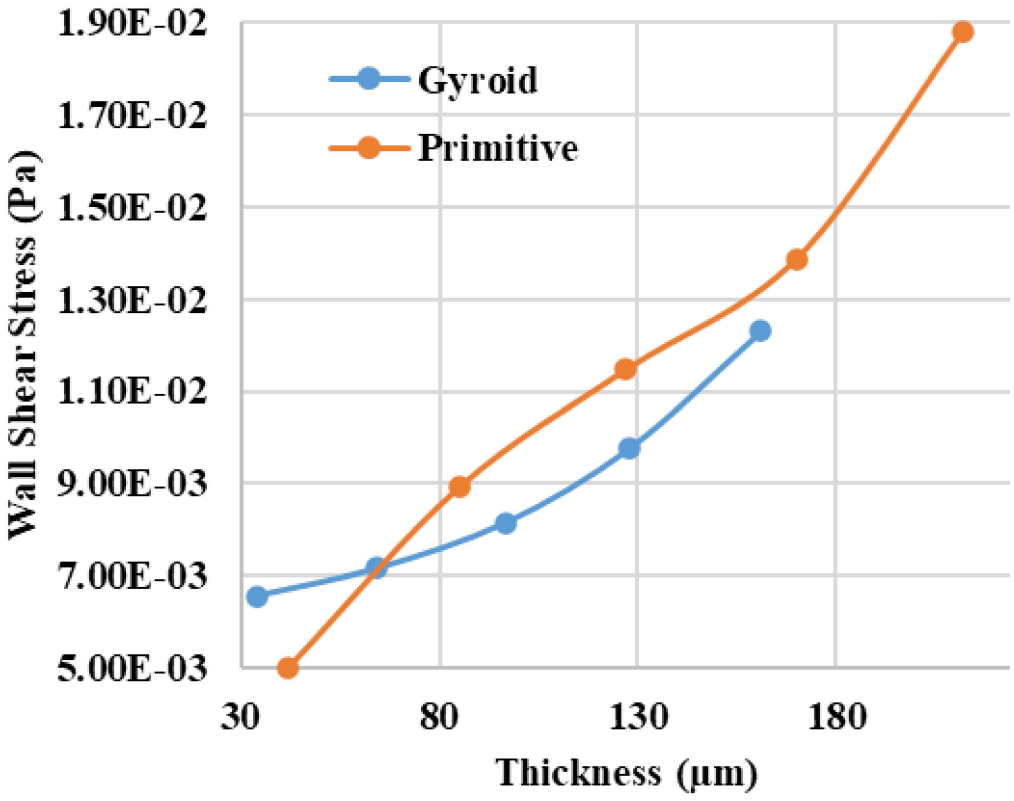

Figure 6.8: Average WSS having 0.1 mm/sec velocity for total developed models on various thickness.

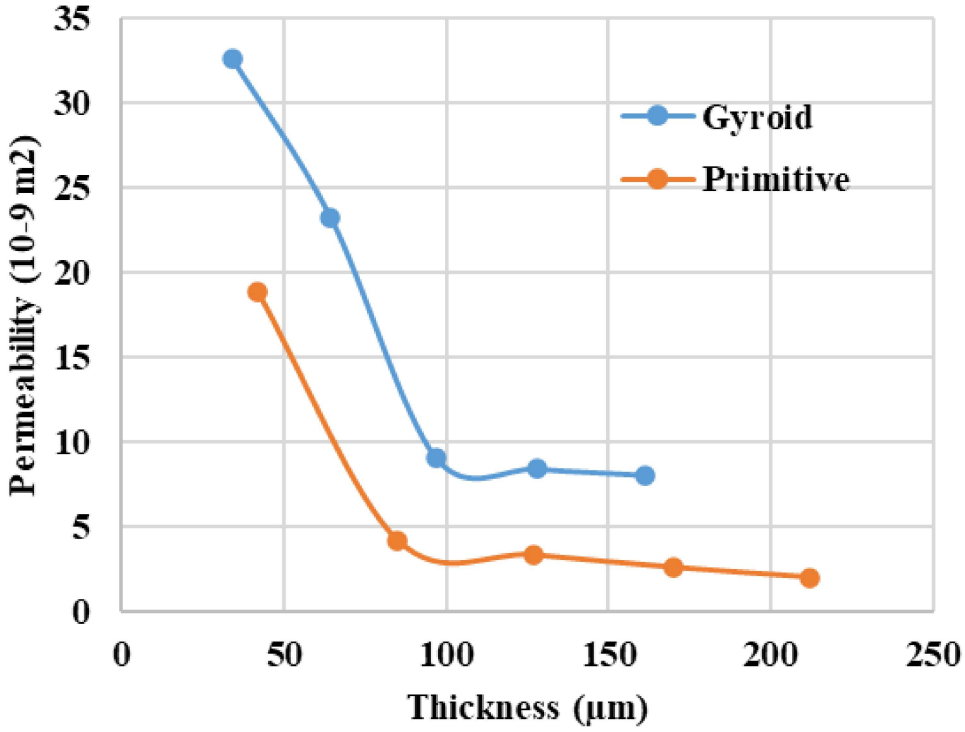

Figure 6.9: Average permeability having 0.1 mm/sec velocity for total developed models.

6.9 Summary

When compared to other periodic surfaces involved in this study, the gyroid model exhibits superior characteristics, as shown by the CFD simulation results. The performance of the two geometries demonstrates that the Wall Shear Strain Rate increased by decreasing pore sizes and decreased by decreasing wall thickness. As the geometrical porosity increases, the permeability improves for both models. Gyroid structures have a more uniform change in permeability with low wall thickness ranges. The primitive structure's thickness variance presents the least significant variability. However, in view of the superior performances of the primitive model in mechanical and morphological analysis and the results presented here, the range of permeability has a good correlation with the experimental study performed by Li et al 2009 (Li et al. 2009, Olivares et al.2009, Zhao et al. 2015). Hence, the primitive model can be

recommended for the development of porous implants for this particular work. However, using other structures needs to involve other experimental studies for deterministic inclusions.